Thin film composite hollow fibre forward osmosis membrane module for the desalination of brackish groundwater for fertigation

Fezeh Lotfi[1], Sherub Phuntsho[1], Tahir Majeed[1], Kwonil Kim[2], Dong Suk Han[3], Ahmed Abdel-Wahab[3], Ho Kyong Shon[1,*]

[1]*Centre for Technology in Water and Wastewater, School of Civil and Environmental Engineering, University of Technology, Sydney (UTS), Broadway, NSW 2007, Australia*

[2]*Samsung Cheil Industries Inc., 332 2, Gocheon-Dong, Gyeonggi-Do, Uiwang-Si 437 711, Republic of Korea*

[3]*Chemical Engineering Program, Texas A&M University at Qatar, PO Box 23874, Doha, Qatar*

* Corresponding author. Email: Hokyong.Shon-1@uts.edu.au

Abstract

The performance of recently developed polyamide thin film composite hollow fibre forward osmosis (HFFO) membrane module was assessed for the desalination of brackish groundwater (BGW) for fertigation. Four different fertilisers were used as draw solution (DS) with real BGW from the Murray-Darling Basin in Australia. Membrane charge and its electrostatic interactions with ions played a significant role in the performance of the HFFO module using fertiliser as DS. Negatively charged polyamide layer promotes sorption of multivalent cations such as Ca^{2+} enhancing ion flux and membrane scaling. Inorganic scaling occurred both on active layer and inside the support layer depending on the types of fertiliser DS used resulting in severe flux decline and this study therefore underscores the importance of selecting suitable fertilisers for the fertiliser drawn forward osmosis (FDFO) process. Water flux under active layer DS membrane orientation was about twice as high as the other orientation indicating the need to further optimise the membrane support structure formation. Water flux slightly improved at higher crossflow rates due to enhanced mass transfer on the fibre lumen side. At 45% packing density, HFFO could have three times more membrane area and four times more volumetric flux output for an equivalent 8040 cellulose triacetate flat-sheet FO membrane module.

Keywords: desalination, forward osmosis, fertigation, hollow fiber membrane, fertiliser drawn forward osmosis, fertigation

1. Introduction

Many countries are now facing acute water scarcity problems and the impact of climate change is further worsening the water crisis [1]. With the rapid increase in the world's population, the water demand is all set to increase further indicating that the water crisis is going to become even more severe in the future. Desalination is therefore going to play an increasingly significant role in solving the water crisis [2, 3]. There are several state-of-the-art desalination technologies however, all these technologies are capital and energy intensive process [4] making desalination either unaffordable or not a cost-effective option especially

for large-scale irrigation purpose. Agriculture sector account for 70% of the world's total water consumption [5] and therefore water shortage could have a devastating consequences on the world's food security [1]. Reverse osmosis (RO) process is currently the most energy efficient desalination technology [6] however; it remains unaffordable to many societies in the world and certainly not for irrigation use. The high capital and operating costs associated with the RO technology is because of the need to operate the process at a high hydraulic pressure [7, 8].

Recently, there have been efforts to develop alternative desalination technologies that operate at low or no hydraulic pressure and potentially reduce the capital and operation costs. Forward osmosis (FO) process has emerged as one of the most promising candidates for desalination with a potential to consume much lower energy than the conventional processes depending on the types of applications [9, 10]. The FO process relies on the osmotic pressure difference across the semi-permeable membrane as the driving force to separate salt from the saline water sources instead of hydraulic pressure in the RO process. The osmotic driving force is generated by using a concentrated draw solution (DS) on one side of the osmotic membrane and feed solution (FS) or the impaired water such as saline water on the other side of the membrane. The water moves from the lower concentrated FS towards the higher concentrated DS by natural osmosis due to osmotic pressure difference without using any external energy. The DS finally becomes diluted but it cannot be used directly for potable purpose unless the draw solute is separated and removed from the pure water. A post-treatment process is essential for the FO process which could still require energy. Finding an ideal draw solute for FO process is therefore still a big challenge at the moment for potable water desalination.

FO is however found ideal when the presence of draw solutes adds value and as such the diluted DS can be applied directly without the need to separate the draw solutes from the water [11]. Fertiliser drawn forward osmosis (FDFO) process is one of such application in which saltwater is converted into nutrient rich water for fertigation using fertiliser solution as DS. The FDFO process has been recently recognised and studied as one of the most practical applications of FO process for irrigation [12, 13]. Since the fertiliser is needed for the growth of the crops/plants, the question of separation of draw solutes from pure water does not arise unlike for the potable water purpose. The fertiliser concentration however must meet the nutrient standards for direct fertigation and this is challenging especially when feed water with a higher salinity is used. Few options have been explored to reduce the fertiliser concentration such as using blended fertiliser as DS [12], using nanofiltration (NF) as either pre-treatment to reduce feed TDS or as post-treatment process to reduce fertiliser concentration and recycle the excess fertiliser for further reuse and extraction of water [14].

Membrane properties play a major role in the performance of the FO process [9, 15, 16]. Following a renewed research interest in the FO process for various applications recently, many new high performing FO membranes have been reported [17-19]. Most efforts however focussed on developing polyamide (PA) based thin film composite (TFC) flat-sheet FO membranes with highly porous support layer to reduce the dilutive internal concentration polarisation (ICP), found mainly responsible for lower flux efficiency in the FO process. Although these efforts have helped improve the water flux by several factors however such membranes are also found to have low mechanical strength [20-22]. Although, the FO process does not use hydraulic pressure as the driving force nevertheless, membranes in general have to be robust to endure long-term operations.

Hollow fibre FO (HFFO) membranes could offer several advantages compared to flat sheet FO membranes [23]. Hollow fibre module have much higher membrane area to volume ratio

than flat sheets so that large membrane area can be packaged into a small volume (high packing density) thereby decreasing the footprint and capital cost. For thin membranes without a fabric backing, fibres are self-supporting and less susceptible to damage during operational process [24]. As a result of their rugged self-supporting geometry, HFFO membranes can be made with thinner substrates without fabric backing thereby not only reducing the material cost but also in reducing the ICP effects. Lab-scale HFFO investigation during our recent study [25] concluded that water flux during HFFO comparatively gave up to 66% higher flux outcome in comparison of flat sheet membrane using fertilisers as DS. Most studies on the FO process including the FDFO process were however conducted at a lab-scale level with a very small membrane area, mostly less than 0.05 m^2 using the only commercialised cellulose triacetate (CTA) FO membrane and hence the study using hollow fibre FO membrane module at a larger-scale level are still very limited.

This study investigates the performance of the recently developed PA TFC HFFO membrane module for the desalination of real brackish groundwater (BGW) for irrigation using fertiliser as DS. This is the first study on the FDFO desalination process using PA HFFO membrane module at a much larger scale level than the lab-scale level reported in many earlier studies. The other specific objectives are to evaluate how the solution properties such as FS and DS properties and operational conditions such as crossflow rates, membrane orientation influence the performance of the HFFO when operated at a larger-scale module level. The study also investigated the impact of scaling on the HFFO membrane when fertilisers are used as DS with the real BGW for desalination. It is important to note here that, the scope of this study is limited to evaluating the performance of the newly developed HFFO membrane module for the FDFO desalination process. The post-treatment system to meet the water quality standard in terms of nutrient concentration required for fertigation of crops is not included in this study as it has been separately studied earlier [13, 26, 27].

2. Materials and methods

2.1 **Draw solution and feed solution**

The saline FS was prepared by dissolving the actual BGW salt in the tap water (TW). The BGW salt supplied by Pyramid salt Pty. Ltd Australia is collected from some of the evaporation ponds that are part of the salt interception scheme located within the Murray-Darling Basin in Australia [13]. The detailed composition of the BGW salt is presented in Table 1. To simulate the variation of BGW salinity within the basin [26, 28], feed water containing different levels of salt concentrations or total dissolved solids (TDS) were prepared and used in this study. BGW5, BGW10, BGW20 and BGW35 therefore represent the feed water with TDS of 5, 10, 20 and 35 gL^{-1} respectively.

Table 1: Composition of raw BGW salt (1 g dissolved in clean water) obtained from the evaporation ponds of the salt interception scheme within the MDB. This same salt was used to prepare FS of different concentrations by dissolving in the distilled water. The list provides only those major elements.

Four different fertilisers were used as draw solutes which included monoammonium phosphate or $NH_4H_2PO_4$ (MAP), diammonium phosphate or $(NH_4)_2HPO_4$) (DAP), ammonium sulphate or $(NH_4)_2SO_4$ (SOA) and calcium nitrate or $Ca(NO_3)_2.4H_2O$. The selection of the fertilisers were based on the earlier studies in which these fertilisers were found to be suitable for use as DS [12, 13]. NaCl was also used as reference draw solutes to compare the performance of the HFFO membrane module with available literatures on the HFFO membranes. All chemicals used in this study were of technical grade (Chem Supplies, Australia). All the initial fertiliser DS were prepared by dissolving the fertiliser salts in distilled water. Table 2 shows some of the essential properties for the five selected fertiliser DS in solution.

Table 2: Basic and essential properties of the five selected DS used in this study. The speciation data was obtained using OLI Stream Analyser 9.1.

2.2 HFFO module experimental setup and operating procedures

The process layout diagram of the semi-pilot scale FO unit is presented in Figure 1 along with the picture of the setup used in the lab. The housing of the HFFO element had an internal diameter of 7.5 cm and length of 50 cm. The element was composed of 790 individual fibres with an effective length of 45 cm and a total membrane area of 1 m^2 supplied by Samsung Cheil Industry, South Korea. The fibres were glued together at each end of the housing element to provide a perfect sealing and to prevent the leakage of solutions. The lumen side of the fibre was composed of PA TFC active layer supported on the porous polyethersulfone (PES) hollow fibre substrate on the outer shell of the fibre. The inner and outer diameters of these hollow fibre membranes were 0.9 and 1.2 mm, respectively. The pure water permeability coefficient of the HFFO membrane determined in RO mode at test pressure ranging between 1.0 and 2.0 bar was 1.92±0.11 $Lm^{-2}h^{-1}bar^{-1}$ while the NaCl (500 mg/L) rejection was 98.5% at 2 bar. Table 3 provides summary of information on the HFFO membrane and the its module used in this study.

Two discharge pumps one each for DS and FS were used to maintain cross flows within the HFFO membrane module. The FS flowed inside the lumen of the HFFO while the DS flowed outside of fibre through the housing, unless stated otherwise. Unless stated otherwise, most experiments were conducted at a flow rate of 6 L/min and under a counter-current crossflow mode and these translate to crossflow velocities of 19.9 cm/s and 2.8 cm/s inside the fibre and outside the fibre, respectively. The flow rate of 6 L/min was the maximum that could be achieved with the two pumps used in this study and since these pumps were not variable speed drive pumps, the maximum flow rate was therefore used for all the experiments. The experiment for crossflow rate at 2.5 L/min (8.3 cm/s inside the fibre and 1.2 cm/s outside the fibre) was however conducted using a bypass to control the flow rate to the hollow fibre module. The initial volume of the DS used was 5.0 L and the FS was 100 L. All the experiments were conducted in a batch mode in which both the solutions, after passing through the membrane, were returned or recycled back to their respective tanks. This led to the continuous dilution of the DS and a continuous increase in the concentration of the FS, resulting in a decrease in water flux over time.

The performances of the HFFO membrane module were assessed in terms of water flux and the loss of draw solutes by reverse solute flux (RSF). Water flux across the membrane in the FO process was calculated from the change in the volume of the DS in the DS tank with the help of a digital mass scale (GFK 300, ADAM) connected to a computer for online data logging. The RSF was evaluated by recording the increase in the conductivity of the feed water by using TW as feed. Since the same HFFO membrane module was used for all the experiments, it was important that the membrane scaling and fouling from the earlier experiments, if any, did not affect the results of the subsequent experiments. Therefore, a strict membrane cleaning protocol was adopted in this study after each experiment. After each experiment, the membrane was physically cleaned by replacing both DS and FS with TW and by providing high cross flow rates (6 L/min, limited by the pump capacity) for about 30 minutes. The baseline flux was determined (using 1.0 M NaCl as DS and TW as FS under the similar operating conditions described above) after each experiment to ensure that the water flux for the HFFO membrane module is fully restored before starting the next experiment. If complete recovery was not observed, acid cleaning was performed using 0.1 N HCl for 15 minutes to ensure that flux was almost fully recovered before starting the next experiment. Most FO experiments were repeated to confirm the accuracy of the data obtained and most of flux data were found to be within the error range of 3 to 7%. Some of the experiments were repeated three times especially when some unusual results were obtained. Wherever applicable, the error bar has been provided for each data such as in the Figures.

Figure 1. Experimental setup for the FDFO desalination process using hollow 1 m^2 HFFO membrane module. (a) Picture of the HFFO membrane module used for all FO experiments in the lab and (b) the schematic layout of the FDFO desalination process.

Table 3: Basic information about the HFFO membrane and the membrane module used in this study

3. Results and discussion

3.1 Performance of HFFO membrane module under different draw solution and feed solution conditions

The solution properties play a significant role in the performance of the FO process [14, 16, 29]. The performances of the HFFO membrane module under different solution properties were evaluated using different types of DS, different DS concentrations and different feed TDS. The performance of the HFFO module was measured in terms of the variation of water fluxes as a function of cumulative volume of water extracted during the FO process. The HFFO membrane module was operated in a batch mode which led to continuous dilution of the DS and continuous increase in the TDS of the FS with increase in the cumulative volume of water extracted as explained earlier under Section 2.2. DS concentration or the osmotic pressure of the DS is the main driving force in the FO process and a continuous decrease in the concentration could therefore result in flux decline with time or cumulative volume which must be identified from the flux decline due to membrane scaling or fouling. In addition, the TDS of the FS also increases with time as more and more water permeates through the

membrane towards the DS with time which could also contribute towards gradual flux decline. The osmotic pressures of the five DS at 1 M and 2 M concentrations are provided in Table 2. The variations of the osmotic pressure with the concentration for the five DS can be found elsewhere [13]. Therefore the performances of the HFFO membrane module are all compared in terms of the variation in the water flux with cumulative volume of extracted water instead of traditional approach of comparing the flux variations with the operating time. The water flux versus operation time as used in most of the earlier studies for FO process in fact does not provide adequate comparison because of the differences in the extent of dilution of the DS as the DS is recycled back to the DS tank.

The performances of the HFFO membrane module using four different types of DS with BGW5 as FS is presented in Figure 2(a) and the results show that, SOA and NaCl have the highest water fluxes amongst the five DS tested in this study. The osmotic pressures of the SOA and NaCl are comparable for concentrations up to 1.0 M (beyond 1 M NaCl shows higher osmotic pressure) [13] (also refer Table 2). Although the osmotic pressures or the driving forces of the CAN and DAP are higher than SOA, NaCl and MAP at 1 M concentration nevertheless, their water fluxes are much lower and in fact, even lower than MAP with the lowest osmotic pressure. While DAP usually showed lower water fluxes in our earlier studies too with CTA FO membrane [13, 28], nevertheless the lower and sharp decline in water fluxes for DAP and CAN with HFFO membrane is unique to this study. Since a gradual flux decline with cumulative volume or time is naturally expected for a batch mode of FO operation however, the sharp flux decline observed for DAP and CAN is in deviation from this normal flux decline, which is therefore worth further discussing.

The rapid flux decline for CAN and DAP as DS is likely due to membrane scaling as explained below. To confirm that scaling had indeed occurred during the FDFO process in Figure 2(a), baseline fluxes of the HFFO membrane module were determined immediately after each experiment (before physical cleaning) using 1 M NaCl as DS and TW as FS. The results in Figure 2(b) show that, the baseline fluxes for the HFFO membrane module after experiment with any of the five DS did not fully recover to its initial baseline flux indicating that scaling had indeed occurred during experiments with all five DS although the severity of scaling is different. After physical cleaning for 30 minutes using TW at 6 L/min (crossflow velocities of 19.9 cm/s inside the fibre and 2.8 cm/s outside the fibre), the water flux recoveries were almost 100% for NaCl, SOA, CAN and MAP indicating that the scaling might have occurred on the active layer side of the membrane facing the FS. This scaling on the active layer side of the HFFO membrane facing the FS could be due to two possible reasons: super saturation of feed ions or reverse diffusion of draw solute ions that could interact with the feed ions or both. It has been reported in many earlier studies that, organic fouling or inorganic scaling formed on the active layer side of the membrane could be cleaned simply by physical cleaning and seldom required chemical cleaning [30, 31]. The poor flux recovery of the HFFO membrane module by physical cleaning after DAP experiment and therefore indicates that, scaling must have occurred inside the support layer side of the HFFO membrane, which is immune to physical cleaning. Chemical cleaning of the HFFO membrane module was however able to fully recover the water flux. The scaling phenomenon in the HFFO membrane module is explained as follows.

The flux decline with CAN as DS is likely due to the reverse diffusion of the CAN DS towards the FS, which then interacts with scaling ions such as SO_4^{2+} to form $CaSO_4$ or gypsum. The reverse diffusion of CAN is generally reported to be higher than other DS containing divalent cations [32, 33]. The major species present in the CAN DS are Ca^{2+} and

NO_3^- as presented in Table 2. The rate of reverse diffusion is a complex phenomenon involving membrane properties, solute properties and solution chemistry. NO_3^- has one of the lowest hydrated ionic radii because of which the rate of reverse diffusion is high compared to other anions. Since NO_3^- has high rate of reverse diffusion, Ca^{2+} ion must also permeate at similar rate to maintain membrane electro-neutrality. The hydrated ionic radius of the Ca^{2+} ions are much larger than nitrate NO_3^- ions and hence its easy passage through the membrane will be restricted however, since the PA rejection layer is negatively charged, it would also promote sorption of Ca^{2+} ions on its membrane interface which could eventually lead to permeation of some of the Ca^{2+} ions through the membrane. The PA active layer of the TFC membranes is usually negatively charged due to the presence of carboxylic functional groups [34, 35] that could form complexes particularly with the divalent ions such as Ca^{2+} and Mg^{2+} This high reverse diffusion of CAN is evident from the results presented in Figure 6 using TW as FS (more discussion on Figure 6 is included later part of this section) although the mechanism involved in this particular case is the solution diffusion model due to the absence of ions in the FS. This reverse permeation or diffusion of Ca^{2+} ions towards the FS could therefore result in the formation of $CaSO_4$ or gypsum scales by combining with SO_4^{2+} ions present in the FS (refer Table 1 for FS composition). Although the other anions are also present on the BGW FS however, SO_4^{2-} with larger valency could have higher affinity towards Ca^{2+} ion than the other monovalent anions. As the concentration of Ca^{2+} ions at the membrane surface increases with time, it could initiate the formation of gypsum pre-nucleation cluster (since $CaSO_4$ has very low solubility) and then gradually resulting in surface crystallisation on the PA active layer [30]. Scaling of FO membrane with CAN as DS using CTA membrane was not observed in our earlier studies [28] because CTA membranes are generally not charged at neutral pH and hence reverse diffusion of CAN is expected to be lower than negatively charged PA membrane.

Similar sharp flux decline was observed with the DAP as DS as shown in Figure 2(a). A significant scaling problem was experienced with DAP DS using CTA membrane in our earlier studies due to reverse diffusion of phosphate ions that formed calcium phosphate scales at the active layer side of the CTA membrane [28]. The scaling mechanism however could be slightly different here with the HFFO membrane because of the negatively charged PA layer that determines the ion transfer across the membrane and in particular the scaling precursor ions. One of the major ionic species of the DAP is NH_4^+ and with its very low hydrated ionic radius, NH_4^+ could easily diffuse through the membrane. The reverse diffusion of NH_4^+ ions may be further facilitated by the negatively charged membrane surface through sorption of NH_4^+ ions that could accelerate diffusion. To maintain electro-neutrality, the phosphate anions may be compelled to diffuse at the similar molar flux rate as NH_4^+. Phosphate ions are generally multivalent anions (refer to Table 2 for species) and hence the reverse diffusion through the negatively charged membrane will not be as fast as NH_4^+ since its permeation will be restricted due to charge exclusion of the multivalent phosphate anions.

The previous study has suggested two transport mechanisms for solute permeation in the FO process: solution diffusion and ion-exchange mechanisms [32]. In the solution-diffusion mechanism, an anion and cation from the FS or DS permeates together in equal molar concentrations to maintain membrane electro-neutrality. In ion-exchange mechanism however, the ion from FS exchanges with the ion from the DS. It is apparent from Table 1 that, significant concentrations of Na^+, Ca^{2+} and Mg^{2+} ions are present in the BGW FS. The negatively charged PA active layer of the membrane could promote sorption of cations present in the FS eventually facilitating forward diffusion of cations including Ca^{2+} and Mg^{2+}

through the PA layer to compensate the high rate of NH_4^+ permeate towards the FS. The permeation of Ca^{2+} or Mg^{2+} ions or both from the FS towards the DS containing phosphate ions could form phosphate scaling (such as calcium phosphate, magnesium phosphate and struvite) inside the membrane support layer that might have contributed to sharp flux decline. The slightly alkaline pH (measured 7.9 at 1 M as presented in Table 2) of the DAP solution could act as a favourable condition for calcium phosphate scale formation inside the membrane support layer [36]. While it is possible that both Ca^{2+} and Mg^{2+} could contribute to the scaling as observed in our earlier study using CTA membrane however, given the higher Ca^{2+} ion concentration than Mg^{2+} in the BGW FS (refer to Table 1), it is reasonable to expect that calcium phosphate could have been contributed more to scaling inside the membrane support layer than magnesium phosphate. Moreover, Ca^{2+} ion rejection is slightly lower than Mg^{2+} ions for PA membranes since Mg^{2+} ions have slightly larger hydrated radius [37].

It may be mentioned here that, gypsum and phosphate scaling could be confirmed by conducting membrane autopsy such as using SEM imaging, EDX or HRD. Autopsy was not conducted in this study because; the manufacturer could supply only one hollow fibre module at this stage and hence the same module had to be preserved for other future studies. The gypsum and phosphates (Mg/Ca) scaling due to reverse diffusion of sulphate and phosphate ions was however already confirmed in our earlier study using SEM imaging, EDS and XRD analysis for similar DS and FS conditions [28] and hence the similar scaling phenomenon is expected to occur in this study.

It may also be argued here that, similar scaling effect as DAP inside the support layer should have been observed when SOA and MAP are used as DS. The forward diffusion of Ca^{2+} ions from the FS could meet similar fate with the sulphate or phosphate ions of the DS inside the support layer resulting in the formation of gypsum or calcium phosphate scaling inside the support layer however, scaling does not seem to have occurred with SOA or MAP as evident from the gradual flux decline observed in Figure 2(a) which is simply due to dilution effect. This could probably be explained due to low pH of the SOA (pH 5.4) and MAP (pH 3.9) DS which likely prevented or perhaps slowed down the formation of scales inside the support layer. Under acidic conditions, the solubility of the inorganic scaling compound is generally enhanced and this is actually the reason why acidic cleaning is generally recommended for removing the scales from the membranes [38]. These results using four different fertiliser DS show that, besides the valency and type of charge of the ions of both DS and FS, the solution pH and membrane charge could play a significant role in the formation of inorganic scales in the FO process and contribute towards flux decline. This results therefore underscore the importance of selecting an appropriate fertiliser DS for the FDFO process for the desalination of BGW for fertigation which otherwise scaling will become a major issue during the process needing chemical cleaning to recover the water flux of the HFFO membrane as evident from the baseline results presented in Figure 2(b).

Figure 2: Performance of the HFFO membrane module under different DS properties. (a) Variation of water fluxes for five different types of DS with cumulative volume of water extracted and (b) baseline fluxes of the HFFO membrane module conducted using 1 M NaCl as DS and TW as FS after the module was subjected to five hours of experimental run with 1 M DS and BGW5 FS.

The performance of the HFFO membrane module under different DS concentrations is presented in Figure 3 for SOA and NaCl as DS using BGW5 as FS. Figure 3(a) shows the variations of water fluxes with cumulative volume using four different concentrations of SOA DS with BGW5 as FS while Figure 3(b) shows the initial water fluxes under different SOA and NaCl DS concentrations with BGW5 as FS. These results show that, the initial water flux of the HFFO module increases when a higher initial DS concentrations are used. This increase is as expected given that at higher concentrations, the DS generates higher osmotic pressure and increases the osmotic driving force resulting in higher water flux. However from Figure 3(b), it is clear that, increase in the water flux gradually levels off at certain value despite further increase in the DS concentration. As observed in the earlier studies, the logarithmic increase in the water fluxes with DS concentrations shown in Figure 3(b) is because of the increased severity of dilutive ICP effects that occur when higher DS concentrations are used. This is the flux paradox of the FO process where, the increased water flux itself acts as a limiting factor by enhancing the dilution of the DS at the membrane surface facing the DS ultimately decreasing the osmotic driving force and the water flux [39, 40]. Using higher DS concentration in fact results in increased feed recovery rate which could promote scaling on the membrane surface however, the results from Figure 3(a) do not show a rapid and unusual flux decline indicating the absence of scaling even when the FO process was operated at higher feed recovery rates. Although the feed recovery rates of the module was less than 3% as mentioned earlier however, the overall feed recovery rate for the FO process conducted in batch mode was as high as 30% for 3 M SOA DS. This result further confirms earlier assumption that using SOA as DS with BGW did not show any sign of significant membrane scaling.

Given the non-linearity of the water flux with the DS concentrations in the FO process, it is important to start the FO process with optimum initial DS concentration. Using a very high DS concentration may in fact increase the pumping cost because of the increase in the specific weight and viscosity of the DS. Moreover, for a full-sale FO desalination plant with fixed number of membrane modules/membrane area, using higher initial DS concentration could also result in higher concentration of the final diluted DS exiting from the modules which is not desirable [41]. Although the DS will ultimately become diluted as the FO process progresses with time, it is important that an optimum initial DS concentration is determined for effective operation of the FDFO desalination process that may also be influenced by factors such as the initial water flux of the DS, total membrane area used in a module, feed properties, etc. The results from Figure 3(b) however cannot identify the optimum initial DS concentration since the module used in this study had an area of only 1 m^2 where the recovery ranges within the module is only about 3%. Experimental data using much larger membrane area or number of modules could provide a more realistic idea of the optimum initial DS concentrations that must be used for the FO process.

Figure 3: Performances of the HFFO membrane module under different DS concentrations. (a) variation of water flux with cumulative extracted volume for different SOA DS concentrations using BGW5 as FS and (b) variations of the initial water fluxes of SOA and NaCl at different DS concentrations using BGW5 as FS. Other experimental conditions include crossflow rate of 6 L/min (crossflow velocities of 19.9 cm/s inside the fibre and 2.8 cm/s outside the fibre), counter-current crossflow mode and operational temperature of 25ºC.

FS properties play a vital role in the performance of the FO process just as they do in the RO process [14]. While the feed salinity or the osmotic pressure of the FS directly influences the net osmotic pressure or the driving force, the presence of other solutes either in dissolved form or in suspended form can directly affect the performance of the FO process. The enhanced concentrations of some of the ions such as Ca^{2+}, SO_4^{2-}, Ba^{2+}, CO_3^{2-}, etc. could be a precursor to scale formation that could lead to rapid flux decline during the membrane process. In order to study the influence of feed TDS on the performance of the HFFO membrane module, five different feed concentrations or TDS were tested using 1 M SOA as DS. These feed conditions are represented as BGW 5, BGW 10, BGW 20 and BGW 35 corresponding to TDS of 5,000, 10,000, 20,000 and 35,000 mgL^{-1} respectively, as FS and 1 M of SOA as DS.

The results in Figure 4(a) show that, the water flux decreases significantly and exponentially with the increase in feed TDS. This decrease in the water flux with TDS is due to increase in the osmotic pressure of the FS that reduces the net driving force or the osmotic pressure difference between the two solutions to generate water flux. The significance of this is that, the volume of water a unit mass of the fertiliser DS can extract will be severely limited by the TDS or osmotic pressure of the FS which will then affect the extent of final dilution or concentration of the diluted fertiliser DS. Using a FS with higher TDS will result in corresponding higher concentrations of the final diluted DS based on the principle of osmotic equilibrium and hence the fertiliser concentration may be too high for direct fertigation [41]. This however applies to any types of FO membranes irrespective of their flux efficiency and their modular configurations. Figure 4(b) shows the variation of water flux with the increase in the cumulative volume using different TDS of the FS 1 M SOA as DS. As the Figure shows, no abrupt decrease in the water flux was however observed during the operation of the FO process indicating that the influence of membrane scaling was not significant in this particular study with SOA DS. This was perhaps due to low recovery rate at which the feed was operated. The final recoveries of the feed water tanks were only about 20% to 30%. Scaling issues could however become more prominent if the unit was operated at higher recovery rates for longer time as a result of surface crystallisation [42, 43].

Figure 4. Influence of feed water properties on the water flux. (a) variation of the initial water flux with the feed TDS and (b) variation of water flux with the cumulative DS volume. Experimental conditions include DS: 5 L of 1M SOA, FS: 100 L of actual BGW at different TDS, crossflow velocity: 19.9 cm/s inside the fibre and 2.8 cm/s outside the fibre.

Most polymeric semi-permeable membranes are not an ideal membrane and hence any osmotic processes involve bi-directional movement of the solutes across the semi-permeable membrane [44, 45]. Similar to RO membranes, FO membranes have salt rejection less than 100% which means that certain percentage of feed salts passes through the membrane along with the permeate. In addition, the FO process involves two independent solutions and hence the draw solutes also reversely diffuse towards the feed (in opposite direction to the permeate water flux) and therefore it is important that the performance of the FO process is assessed in terms of the loss of draw solutes by reverse diffusion. The reverse diffusion of draw solutes has serious implications such as economic loss of the draw solutes, which needs replenishment. More significantly, the presence of certain draw solutes could complicate the

FO concentrated brine management due to the potential of some of the DS to cause environmental toxicity [29].

Reverse diffusion of draw solutes is usually measured in terms of the reverse solute flux (RSF) and specific reverse solute flux (SRSF). The RSF refers to the mass of draw solutes that pass through the membrane in a unit membrane and in a unit time while the SRSF refers to the mass of draw solutes that pass through the membrane per unit volume of water that permeates the membrane. In many earlier studies, the RSF has been observed to increase when higher DS concentrations are used which is also consistent with the solution diffusion models suggested for the RSF [28, 46]. However, from the results in Figure 3 above, it is clear that, the water flux is also higher when higher DS concentrations are used in the FO process. Therefore, SRSF (ratio of solute flux to water flux) has been considered as the most accurate way of assessing the reverse diffusion of the draw solutes per unit volume of water extracted by the DS and hence in this study only SRSF has been used for discussion.

Figure 5 presents the loss of the draw solutes measured in terms of SRSF for all the four fertilisers and NaCl at 1 M DS using TW as FS. TW was used as FS for evaluating the RSF. The SRSF of CAN (1.2 gL^{-1}) was observed the highest while DAP showed the lowest SRSF (0.16 gL^{-1}) amongst the five DS studied. In fact, the SRSF of CAN is even higher than NaCl which is surprising given that, SRSF of NaCl is usually observed to be much lower than those multivalent DS using CTA FO membranes. Although CAN is a divalent DS nevertheless, the high SRSF indicates the role of the negatively charged PA membrane that attracts divalent counter ions (cations) thereby slightly enhancing the passage of Ca^{2+} ions as discussed earlier. Although, NO_3^- ions are expected to be rejected by the negatively charged membrane surface however, in order to maintain electro-neutrality across the membrane, NO_3^- anions have to diffuse simultaneously with the Ca^{2+} ions since there are no other significant ions present in the FS (TW is used). The SRSF of SOA, MAP and DAP is quite reasonably low because of the presence of the multivalent anions which are more repelled and rejected by the negatively charged PA layer of the HFFO membrane. The water flux (5 $Lm^{-2}h^{-1}$ at 0.5 M NaCl as DS and BGW5 as FS) and the SRSF of the NaCl (0.5 gL^{-1}) is comparable to the performances of some of the reported studies on the PA based TFC flat sheet FO and HFFO membranes [18] however, the performance is still not as efficient as other reported PA based TFC HFFO membranes [23].

Figure 5: Loss of draw solutes during the operation of the semi-pilot HFFO unit measured in terms of RSF and SRSF for selected DS concentrations using TW as feed water.

3.2 Performance of a HFFO membrane module under different operating conditions

The performance of the HFFO membrane module was evaluated under different operating conditions such as membrane orientation, crossflow direction and the crossflow rates and their results are presented in Figure 6. As any salt rejecting polymeric membranes, the HFFO used in the study is also made up of an asymmetric structure containing a thin PA salt rejecting layer on the thick porous support layer. Membrane asymmetry plays a significant role on the performance of the FO process. The influence of membrane orientation for the semi-pilot HFFO unit was observed by comparing the water fluxes under active layer facing

FS (AL-FS) and active layer facing the DS (AL-DS). Figure 6(a) shows the variation of water fluxes when the HFFO membrane element was operated under two different membrane orientations using 1.0 M SOA as DS and BGW5 as FS. The results indicate that, under the AL-DS of membrane orientation, the water flux is more than twice as high as under the AL-FS of membrane orientation. The water fluxes in the AL-DS are usually higher as observed in many earlier studies with the membrane synthesised in the labs. Such a large difference in water fluxes between the two modes of membrane orientations not only confirms further how the dilutive ICP plays a major role in lowering the water flux in the FO process but also shows how support layer formation of this HFFO membrane contributes to enhanced dilutive ICP effects.

The initial water flux under the AL-FS of membrane orientation for TFC HFFO membrane module is about 8 $Lm^{-2}h^{-1}$ using 1 M SOA as DS and BGW5 as FS (Figure 6) which is comparable to the water flux of 7 $Lm^{-2}h^{-1}$ for CTA flat-sheet FO membrane operated under similar operating conditions (except in total membrane area) [12]. Given that the TFC HFFO membrane has pure water permeability coefficient two times higher (1.8 $Lm^{-2}h^{-1}$) than the CTA flat-sheet FO membrane (1.01 $Lm^{-2}h^{-1}$) [25], it was in fact expected that the, water flux for TFC HFFO membrane could be comparatively higher than the CTA FO membrane. This therefore indicates that, the dilutive ICP effect for the TFC membrane is even higher than the CTA FO membrane and this could likely be due to the support layer property of the TFC HFFO membrane. Figure 7(a) presents the SEM images of the cross section of the HFFO membrane. The support layer of the fibre has a finger-like structure that is purposely designed to create macro-voids and increase the porosity of the support layer and facilitate easier diffusion of DS towards the rejection layer located on the lumen side of the fibre. The support layer should provide minimum resistivity to the diffusion of the DS which otherwise could significantly reduce the driving force to generate water flux. This is one of the main reasons why most recent efforts to develop efficient FO membrane have been in improving the structural parameters such as by increasing the porosity and reducing the tortuosity and thickness so that the dilutive ICP effect is reduced [47, 48]. However, despite higher PWP for the HFFO membrane, its lower water flux than expected under the FO mode indicates that, the resistance to diffusivity of the DS in the support layer is still high. A closer observation of the support structure from the SEM images in Figure 7(a) reveals that, the support layer formation may not have been a fully optimised.

Although, finger-like macro-voids are formed within the support layer, they do not seem to be connected or open to the external shell of the fibre. Most macro-voids, visible in the SEM images, tend to terminate before reaching the external shell of the fibre making the layer near the shell surface appear denser and less porous. This could likely increase the resistivity of the support layer structure to the diffusivity of the draw solutes. The other observation to note is the presence of two distinct layers of support structure formation each having independent finger-like water channel formations not directly connected to each layer formation. There is clearly a solid mass of membrane support layer between the two finger-like layers of porous water channels. This discontinuity of the finger-like water channels within the support layer could reduce the diffusivity of the draw solution significantly thereby likely contributing to the increased severity of dilutive ICP effects in the AL-FS of operation. Such discontinuity of the finger-like water channels were not reported in the PA TFC flat-sheet FO membranes where the water flux under the FO mode of membrane orientation is reported to be comparatively higher [17-19]. Given the propriety of the TFC HFFO membrane used in this study, we could not shed any light on the reasons for the formation of this type of support layer formation. The lower than expected water flux for the TFC HFFO membrane used in

this study however shows the importance of fully optimising the support layer formation during the fabrication of the HFFO membrane.

It may not be however fair to compare the water flux between the CTA and TFC membrane under AL-FS because they have totally different membrane properties in terms of materials, surface chemistry, salt rejection layer thickness, support layer structure, etc. which all could result in different efficiencies. This finger-like support structure for TFC HFFO membrane is quite different from the one generally shown cross section of the flat sheet CTA FO membrane composed of polymer mesh embedded within the CTA membrane reported in many literatures [17-19]. Comparison under the AL-DS of membrane orientation between HFFO membrane and flat sheet CTA FO membrane is however straightforward given that the dilutive effect now occurs on the external side of the membrane. By safely neglecting the contribution of concentrative ICP effects, which is generally less significant than the dilutive ICP effect, the comparison now becomes only due to a function of the membrane active layer properties of the two membranes.

The percentage increase in the water flux under the AL-DS compared to AL-FS of membrane orientation for HFFO membrane is significantly higher than that of the CTA FO membrane [14]. This high water flux under the AL-DS of membrane orientation for TFC HFFO membrane is likely due to two main factors: high water permeability and enhanced DS mixing on the lumen side. The water flux is a function of the membrane permeability and driving force and since the PWP of TFC HFFO membrane is much higher than the CTA FO membrane, its water flux under the AL-DS is therefore expected to be much higher. The other likely reason is the high velocity shear of the DS that occurs within the small confined tube of the lumen side of the HFFO membrane favouring more turbulence and better mixing and hence, lower dilutive ECP effects. The Reynolds number of the DS inside the lumen side (PRO) of the hollow fibre membrane was 84,140 compared to only 13,360 when it flows outside the lumen under the AL-FS of operation which could significantly enhance the mixing thereby reducing the dilutive ECP effects. Such conditions are not available when the DS flows outside of the lumen side of the HFFO membrane where the spacing or the cross sectional area is comparatively large and hence the DS velocity could be much lower than lumen flow for the same DS flow rates. The high water flux under the AL-DS of operation for this HFFO membrane is quite promising especially when a high quality pre-treated feed water is to be used for the desalination process [26].

Crossflow direction could play a significant role in the performance of the FO process both in terms of the water flux and the final concentration of the diluted DS [41]. The influence of the crossflow directions on the semi-pilot HFFO unit was assessed by operating the unit under co-current and counter-current crossflow modes using 1 M SOA as DS and BGW5 as FS. Figure 6(a) shows the variations of the water flux under the two different crossflow modes of operation. It is clear from these results that there are no noticeable differences in water flux between the co-current and counter-current crossflow modes of operations [49]. This is likely due to the short membrane length (45 cm) and the smaller membrane area (only 1 m^2) used in the membrane module which gives a feed recovery rate of only about 3% not adequate to show any noticeable differences in the water flux. FO modelling has in fact shown that, the water flux under the counter-current crossflow mode could be slightly higher than the co-current crossflow mode when the FO process is operated under full-scale modular FO system [41]. Few lab-scale studies using flat-sheet FO membranes have reported a slightly enhanced water flux under the counter-current crossflow mode of operation [49-51].

Figure 6(b) presents the influence of crossflow rates on the water flux. The same crossflow rates were maintained for both the DS and FS although it does not translate into equal crossflow velocity or Reynolds number due to the difference in the geometry for inside and outside the lumen side of the hollow fibre membrane. The influence of the crossflow rates on the water flux of the HFFO membrane module was observed by operating the FO module under two different crossflow rates (2.5 L/min and 6.0 L/min corresponding to Reynolds numbers of 5,566 and 13,360, respectively) and under AL-FS membrane orientation mode. The results in Figure 6(b) indicate that an HFFO membrane unit operated at higher solution flow rates could result in slightly improved water flux. Such visible influence is not usually observed in the lab-scale FO unit using a rectangular FO cell [22, 49, 52]. The slightly enhanced water flux observed at higher crossflow rate is likely due to increased crossflow velocity of the FS that increases the mass transfer coefficient of the feed solutes thereby reducing the concentrative ECP effects at the membrane surface. Increased crossflow rate of the DS on the support layer side of the membrane is not expected to have any influence in reducing the ICP effect as it occurs within the support layer. However, it must be noted that, increasing the flow rates however not only reduces the feed recovery rates but also decreases the dilution of the bulk DS concentration and hence DS that comes out of the module will have much higher concentration which is not desirable. Adopting optimum crossflow velocity is also important as increasing flow rates could also increase cost on the pumping energy.

Figure 6: Performance of the HFFO membrane module under the influence of different operating conditions: (a) different membrane orientations and crossflow directions and (b) different solution crossflow rates. Crossflow rate of 6 L/min corresponds to crossflow velocities of 19.9 cm/s inside the fibre and 2.8 cm/s outside the fibre and likewise, crossflow rate of 2.5 L/min corresponds to 8.3 cm/s inside the fibre and 1.2 cm/s outside the fibre.

Figure 7: Cross-sectional SEM images of the two FO membranes (a) PA HFFO membrane used in this study and (b) CTA FO membrane used in our earlier studies.

3.3 Implications of the performances of the HFFO membrane module

Table 4 presents the comparative parameters of the flat sheet spiral wound (8040) CTA FO membrane module (HTI Inc. USA) recently tested in our lab [53] and the 1.0 m^2 HFFO membrane module used in this study. The HFFO membrane module contains a total of 790 fibres (external fibre diameter of 1.2 mm and internal diameter of 0.9 mm and 45 cm effective length) inside a 7.5 cm diameter module/housing with a total packing density of about 20%. The module average water fluxes are 4.5 $Lm^{-2}h^{-1}$ for 8040 CTA FO module [53] and 6.0 $Lm^{-2}h^{-1}$ for the HFFO membrane module both using 1 M SOA as DS and BGW5 as FS. Table 4 shows that, for a membrane module of similar 8040 size, HFFO membrane will have higher effective membrane area of 14.9 m^2 compared to 11.2 m^2 for spiral wound flat sheet FO membrane based on the similar packing density as used in the test module. Although, the total membrane area of 8040 HFFO module (14.9 m^2) is not significantly higher than the 8040 spiral wound module (11.2 m^2) however, given its higher water flux, the

volumetric flux output per module is significantly higher for HFFO module (89.4 $Lh^{-1}module^{-1}$) than the spiral wound CTA module (39.2 $Lh^{-1}module^{-1}$).

Generally for commercial applications, the preferred packing density of the hollow fibre membrane is generally 45-60% [54]. Assuming a packing density of 45%, the total membrane area for 8040 HFFO membrane has been estimated at 35 m^2 which is three times as high as the effective membrane area of the spiral wound 8040 CTA module. At this packing density, the volumetric output per module would increase to 211 Lh^{-1}, which is more than four times higher than the 8040 CTA FO module. These results indicate the inherent advantages of the HFFO membrane module over the spiral wound CTA FO membrane module in terms of much lower footprint and membrane cost for an FO desalination plant. However, it must also be acknowledged that, the calculations for the 8040 HFFO module is based on the module average water flux of the 1 m^2 HFFO membrane module. The actual module average water flux for the HFFO membrane module with larger membrane area would have slightly lower water flux than used here for calculation since the water flux decreases with the packing density of the hollow fibre module [54, 55].

Table 4: Comparative parameters of the hollow fibre FO and spiral would membrane modules for the FDFO process

4 Conclusions

The performances of the newly developed PA based TFC HFFO membrane module with a membrane area of 1 m^2 were tested using four different fertilisers and NaCl as DS and real BGW FS obtained from one of the salt interception schemes in the Murray Darling Basin. The following are the conclusions drawn from this particular study:

- Membrane charge and its electrostatic interactions with the ions played a significant role in the performance of the HFFO module especially when fertilisers containing scaling ions are used as DS. Negatively charged PA layer of the HFFO membrane favoured sorption of multivalent cations such as Ca^{2+} ions which likely enhanced the ion flux through the rejection layer resulting in the formation of scales and flux decline.
- Although slight scaling seems to have occurred for the HFFO membrane module using all five selected DS however, flux decline was more severe with CAN and DAP fertiliser as DS. Scaling occurred inside the support layer of the HFFO membrane when DAP was used as DS and only acidic cleaning was able to restore the flux fully. Physical cleaning was effective for restoring the water flux of the HFFO membrane module when scaling occurred on the active layer side of the membrane. The complex interaction between the membrane surface and the solute ions however underscores the importance of selecting a suitable fertiliser candidate for the desalination of BGW by FDFO process.
- The water flux under the active layer DS (AL-DS) of membrane orientation was about twice as high as under active layer FS (AL-FS) of membrane orientation. The lower water flux than expected in the AL-FS of membrane orientation was probably due to the non-optimised support layer formation in which the finger-like water channels were not fully inter-connected thereby reducing the diffusivity of DS through the support layer.

- Consistent with the lab-scale studies, the water flux increases non-linearly with the increase in the DS concentrations, which underscores the importance of selecting an optimum initial DS concentration to reduce the pumping energy cost.
- The water flux decreased exponentially with the increase in the feed TDS however, no abrupt decrease in the water flux was observed indicating the absence of membrane scaling using SOA was used as DS.
- A slight increase in the water flux was observed when the cross flow rates of the solutions were increased due to enhanced velocity shear and mass transfer on the FS side of the membrane that likely reduced the concentrative ECP effects.
- No significant difference in the water flux between co-current and counter-current crossflow directions was observed probably due to the low recovery rate of this HFFO membrane module.
- Based on the performance of the HFFO membrane module in this study, it is observed that the HFFO membrane module with a packing density of 45% could offer membrane area three times more and volumetric flux output four times more compared to the CTA FO membrane with a size similar to 8040 spiral wound FO membrane module.

Acknowledgements

This study was supported by the National Centre of Excellence in Desalination Australia (NCEDA), which is funded by the Australian Government through the Water for the Future initiative. We would like to thank an ARC Future Fellowship (FT140101208) and Samsung Cheil Industries, Korea for providing hollow fibre FO membrane.

References

1. M. W. Rosegrant, S. A. Cline, Global Food Security: Challenges and Policies, Science 302(2003): 1917-1919.
2. E. Lopez-Gunn, M. Ramón Llamas, Re-thinking water scarcity: Can science and technology solve the global water crisis?, Natural Resources Forum 32(2008): 228-238.
3. M. Elimelech, W. A. Phillip, The Future of Seawater Desalination: Energy, Technology, and the Environment, Science 333(2011): 712-717.
4. M. A. Shannon, P. W. Bohn, M. Elimelech, J. G. Georgiadis, B. J. Marinas , A. M. Mayes, Science and technology for water purification in the coming decades, Nature 452(2008): 301-310.
5. D. L. Shaffer, N. Yin Yip, J. Gilron , M. Elimelech, Seawater desalination for agriculture by integrated forward and reverse osmosis: improved product water quality for potentially less energy, Journal of Membrane Science 415–416, 1 October 2012, Pages 1-8(2012): 1-8.
6. R. Semiat, Energy Issues in Desalination Processes, Environmental Science & Technology 42(2008): 8193-8201.
7. R. K. Mcgovern, J. H. Lienhard V, On the potential of forward osmosis to energetically outperform reverse osmosis desalination, Journal of Membrane Science 469(2014): 245-250.

8. M. Li, Reducing specific energy consumption in Reverse Osmosis (RO) water desalination: An analysis from first principles, Desalination 276(2011): 128-135.
9. S. Zhao, L. Zou, C. Y. Tang , D. Mulcahy, Recent developments in forward osmosis: Opportunities and challenges, Journal of Membrane Science 396(2012): 1-21.
10. T.-S. Chung, X. Li, R. C. Ong, Q. Ge, H. Wang , G. Han, Emerging forward osmosis (FO) technologies and challenges ahead for clean water and clean energy applications, Current Opinion in Chemical Engineering 1(2012): 246-257.
11. L. A. Hoover, W. A. Phillip, A. Tiraferri, N. Y. Yip , M. Elimelech, Forward with Osmosis: Emerging Applications for Greater Sustainability, Environmental Science & Technology 45(2011): 9824–9830.
12. S. Phuntsho, H. K. Shon, T. Majeed, I. El Salibya, S. Vigneswarana, J. Kandasamy, S. Hong , S. Leeb, Blended fertilisers as draw solutions for fertiliser drawn forward osmosis desalination, Environmental Science & Technology 46(2012): 4567−4575.
13. S. Phuntsho, H. K. Shon, S. Hong, S. Lee , S. Vigneswaran, A novel low energy fertilizer driven forward osmosis desalination for direct fertigation: evaluating the performance of fertilizer draw solutions, Journal of Membrane Science 375(2011): 172-181.
14. S. Phuntsho, S. Sahebi, T. Majeed, F. Lotfi, J. E. Kim , H. K. Shon, Assessing the major factors affecting the performances of forward osmosis and its implications on the desalination process, Chemical Engineering Journal 231(2013): 484-496.
15. T.-S. Chung, S. Zhang, K. Y. Wang, J. Su , M. M. Ling, Forward osmosis processes: Yesterday, today and tomorrow, Desalination 287(2012): 78-81.
16. T. Y. Cath, A. E. Childress , M. Elimelech, Forward osmosis: Principles, applications, and recent developments: Review, Journal of Membrane Science 281(2006): 70-87.
17. K. Y. Wang, T.-S. Chung , G. Amy, Developing thin-film-composite forward osmosis membranes on the PES/SPSf substrate through interfacial polymerization, AIChE journal 58(2012): 770-781.
18. J. Wei, C. Qiu, C. Y. Tang, R. Wang , A. G. Fane, Synthesis and characterization of flat-sheet thin film composite forward osmosis membranes, Journal of Membrane Science 372(2011): 292-302.
19. N. Y. Yip, A. Tiraferri, W. A. Phillip, J. D. Schiffman , M. Elimelech, High Performance Thin-Film Composite Forward Osmosis Membrane, Environmental Science & Technology 44(2010): 3812-3818.
20. N. Bui, M. L. Lind, E. M. V. Hoek , J. R. Mccutcheon, Electrospun Nanofiber Supported Thin Film Composite Membranes for Engineered Osmosis, Journal of Membrane Science In Press, Accepted Manuscript(2011).
21. C. Qiu, L. Setiawan, R. Wang, C. Y. Tang , A. G. Fane, High performance flat sheet forward osmosis membrane with an NF-like selective layer on a woven fabric embedded substrate, Desalination 287(2012): 266-270.
22. R. Wang, L. Shi, C. Y. Tang, S. Chou, C. Qiu , A. G. Fane, Characterization of novel forward osmosis hollow fiber membranes, Journal of Membrane Science 355(2010): 158-167.
23. S. Chou, L. Shi, R. Wang, C. Y. Tang, C. Qiu , A. G. Fane, Characteristics and potential applications of a novel forward osmosis hollow fiber membrane, Desalination 261(2010): 365-372.
24. K. Y. Wang, T.-S. Chung , J.-J. Qin, Polybenzimidazole (PBI) nanofiltration hollow fiber membranes applied in forward osmosis process, Journal of Membrane Science 300(2007): 6-12.

25. T. Majeed, F. Lotfi, S. Phuntsho, J. K. Yoon, K. Kim , H. K. Shon, Performances of PA hollow fiber membrane with the CTA flat sheet membrane for forward osmosis process, Desalination and Water Treatment (2013): 1-11.
26. S. Phuntsho, S. Hong, M. Elimelech , H. K. Shon, Forward osmosis desalination of brackish groundwater: Meeting water quality requirements for fertigation by integrating nanofiltration, Journal of Membrane Science 436(2013): 1-15.
27. S. Phuntsho, H. K. Shon, S. Hong, S. Lee, S. Vigneswaran , J. Kandasamy, Fertiliser drawn forward osmosis desalination: the concept, performance and limitations for fertigation, Reviews in Environmental Science and Bio/Technology 11(2012): 147-168.
28. S. Phuntsho, F. Lotfi, S. Hong, D. L. Shaffer, M. Elimelech , H. K. Shon, Membrane scaling and flux decline during fertiliser-drawn forward osmosis desalination of brackish groundwater, Water Research 57(2014): 172-182.
29. L. Chekli, S. Phuntsho, H. K. Shon, S. Vigneswaran, J. Kandasamy , A. Chanan, A review of draw solutes in forward osmosis process and their use in modern applications, Desalination and Water Treatment 43(2012): 167-184.
30. B. Mi, M. Elimelech, Gypsum Scaling and Cleaning in Forward Osmosis: Measurements and Mechanisms, Environmental Science & Technology 44(2010): 2022-2028.
31. E. Arkhangelsky, F. Wicaksana, S. Chou, A. A. Al-Rabiah, S. M. Al-Zahrani , R. Wang, Effects of scaling and cleaning on the performance of forward osmosis hollow fiber membranes, Journal of Membrane Science 415–416(2012): 101-108.
32. G. J. Irvine, S. Rajesh, M. Georgiadis , W. A. Phillip, Ion Selective Permeation Through Cellulose Acetate Membranes in Forward Osmosis, Environmental Science & Technology 47(2013): 13745-13753.
33. Q. She, X. Jin, Q. Li , C. Y. Tang, Relating reverse and forward solute diffusion to membrane fouling in osmotically driven membrane processes, Water Research 46(2012): 2478-2486.
34. J. F. Fernández, B. Jastorff, R. Störmann, S. Stolte , J. Thöming, Thinking in Terms of Structure-Activity-Relationships (T-SAR): A Tool to Better Understand Nanofiltration Membranes, Membranes 1(2011): 162-183.
35. A. E. Childress, M. Elimelech, Effect of solution chemistry on the surface charge of polymeric reverse osmosis and nanofiltration membranes, Journal of Membrane Science 119(1996): 253-268.
36. M. L. Harrison, M. R. Johns, E. T. White , M. C. M., Growth Rate Kinetics for Struvite Crystallisation, Chemical Engineering Transactions 25(2011): 309-314.
37. E. R. Nightingale, Phenomenological Theory of Ion Solvation. Effective Radii of Hydrated Ions, The Journal of Physical Chemistry 63(1959): 1381-1387.
38. N. D'souza, A. Mawson, Membrane cleaning in the dairy industry: a review, Critical reviews in food science and nutrition 45(2005): 125-134.
39. W. C. Lay, J. Zhang, C. Tang, R. Wang, Y. Liu , A. G. Fane, Factors affecting flux performance of forward osmosis systems, Journal of Membrane Science 394(2012): 151-168.
40. Y. Xu, X. Peng, C. Y. Tang, Q. S. Fu , S. Nie, Effect of draw solution concentration and operating conditions on forward osmosis and pressure retarded osmosis performance in a spiral wound module, Journal of Membrane Science 348(2010): 298-309.
41. S. Phuntsho, S. Hong, M. Elimelech , H. K. Shon, Osmotic equilibrium in the forward osmosis process: Modelling, experiments and implications for process performance, Journal of Membrane Science 453(2014): 240-252.

42. Y. Liu, B. Mi, Effects of organic macromolecular conditioning on gypsum scaling of forward osmosis membranes, Journal of Membrane Science 450(2014): 153-161.
43. J.-P. Mericq, S. Laborie , C. Cabassud, Vacuum membrane distillation for an integrated seawater desalination process, Desalination and Water Treatment 9(2009): 287-296.
44. M. Elimelech, S. Bhattacharjee, A novel approach for modeling concentration polarization in crossflow membrane filtration based on the equivalence of osmotic pressure model and filtration theory, Journal of Membrane Science 145(1998): 223-241.
45. J. Su, T.-S. Chung, B. J. Helmer , J. S. De Wit, Understanding of low osmotic efficiency in forward osmosis: experiments and modeling, Desalination 313(2013): 156-165.
46. J. S. Yong, W. A. Phillip , M. Elimelech, Coupled reverse draw solute permeation and water flux in forward osmosis with neutral draw solutes, Journal of Membrane Science 392–393(2012): 9-17.
47. S. Zhang, K. Y. Wang, T.-S. Chung, H. Chen, Y. C. Jean , G. Amy, Well-constructed cellulose acetate membranes for forward osmosis: Minimized internal concentration polarization with an ultra-thin selective layer, Journal of Membrane Science 360(2010): 522-535.
48. K. Y. Wang, R. C. Ong , T.-S. Chung, Double-Skinned Forward Osmosis Membranes for Reducing Internal Concentration Polarization within the Porous Sublayer, Industrial & Engineering Chemistry Research 49(2010): 4824-4831.
49. D. H. Jung, J. Lee, D. Y. Kim, Y. G. Lee, M. Park, S. Lee, D. R. Yang , J. H. Kim, Simulation of forward osmosis membrane process: Effect of membrane orientation and flow direction of feed and draw solutions, Desalination 277(2011): 83-91.
50. R. Hughes, *Industrial membrane separation technology*. 1996: Springer.
51. S.-M. Shim, W.-S. Kim, A numerical study on the performance prediction of forward osmosis process, J Mech Sci Technol 27(2013): 1179-1189.
52. N. Widjojo, T.-S. Chung, M. Weber, C. Maletzko , V. Warzelhan, A sulfonated polyphenylenesulfone (sPPSU) as the supporting substrate in thin film composite (TFC) membranes with enhanced performance for forward osmosis (FO), Chemical Engineering Journal 220(2013): 15-23.
53. J. E. Kim, S. Phuntsho, F. Lotfi , H. K. Shon, Investigation of pilot-scale 8040 FO membrane module under different operating conditions for brackish water desalination, Desalination and Water Treatment doi: 10.1080/19443994.2014.931528(2014).
54. D. Li, R. Wang , T.-S. Chung, Fabrication of lab-scale hollow fiber membrane modules with high packing density, Separation and Purification Technology 40(2004): 15-30.
55. J. Günther, P. Schmitz, C. Albasi , C. Lafforgue, A numerical approach to study the impact of packing density on fluid flow distribution in hollow fiber module, Journal of Membrane Science 348(2010): 277-286.

LIST OF TABLES

Table 1

Composition	Concentrations in 1 gL^{-1} salt solution (mgL^{-1})	Composition	Concentrations in 1 gL^{-1} salt solution (mgL^{-1})
Calcium	32	Chloride	558
Magnesium	13	Sulphate	52
Potassium	3	CO3	2
Sodium	340	Total (TDS)	1000

Table 2

Name of fertilisers	**Chemical formula**	**MW**	**Osmotic pressure at 1M & 2 M (atm)**	**pH*@ 1.0 M**	**Species formed in 2.0 M solution at 25 °C and 1.0 atm. pressure.**
Ammonium sulfate (SOA)	$(NH_4)_2SO_4$	132.1	45.5 & 90.9	5.2	NH_4^+, SO_4^{2-}, $NH_4SO_4^-$
Calcium nitrate (CAN)	$Ca(NO_3)_2$	164.1	51.6 & 107.2	6.8	NO_3^-, Ca^{2+}, $CaNO_3^-$,
Mono-ammonium phosphate (MAP)	$NH_4H_2PO_4$	115.0	43.4 & 86.1	4.2	NH_4^-, $H_2PO_4^-$, $H_2P_2O_7^{2-}$, H_3PO_4, $HP_2O_7^{3-}$
Diammonium hydrogen phosphate (DAP)	$(NH_4)_2HPO_4$	132.1	49.8 & 93.6	7.9	NH_4^+, HPO_4^{2-}, $P_2O_7^{2-}$, $H_2PO_4^-$, $HP_2O_7^{3-}$
Sodium chloride	NaCl	58.44	46.1 & 99.1	7.0	Na^+, Cl^-

Table 3

Membrane parameters	**Values**
Hollow fibre data	
Rejection layer	Polyamide (PA)
Support layer	Polyethersulfone (PES)
Outer diameter	1.2 mm
Inner diameter	0.9 mm
Rejection layer	Inside facing lumen side
Pure water permeability	1.92 ± 0.11 $Lm^{-2}h^{-1}bar^{-1}$
Salt rejection (500 mg/L NaCl)	98.5% at bar 2.0 bar
Module data	
Diameter	7.5 cm
Effective module length	45 cm
Outer module length	50 cm
Total number of fibres	790
Total membrane area	1.0 m2

Table 4

Parameters	**CTA module** [53]	**HFFO module**
Types of module	Spiral wound	Hollow fibre
Module size for comparison	8040= 80" x 40" 20.32 x 101.6 cm	7.5 x 50 cm [used in this study]
Total membrane area	11.2 m^2	1.0 m^2
Module packing volume	$3.2931x10^{-2}$ m^3	$2.2078x10^{-3}$ m^3
Total membrane area converted in 8040 module	11.2 m^2	14.9 m^2 at 20% packing density 35 m^2 at 45% packing density
Module average water flux using [1 M SOA:BGW5]	4.5 $Lm^{-2}h^{-1}$	6.0 $Lm^{-2}h^{-1}$
Volumetric output from each 8040 membrane module	50.4 Lh^{-1}	89 Lh^{-1} at 20% packing density 211 Lh^{-1} at 45% packing density

LIST OF FIGURES


Hollow Fibre Forward Osmosis
Feed Solution
Draw Solution

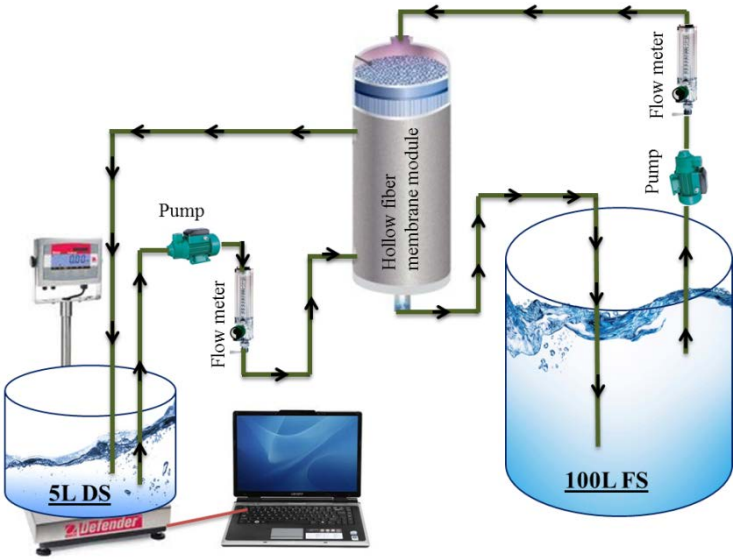
Pump
Flow meter
Hollow fiber membrane module
Flow meter
Pump
5L DS
100L FS

Figure 1

Figure 2

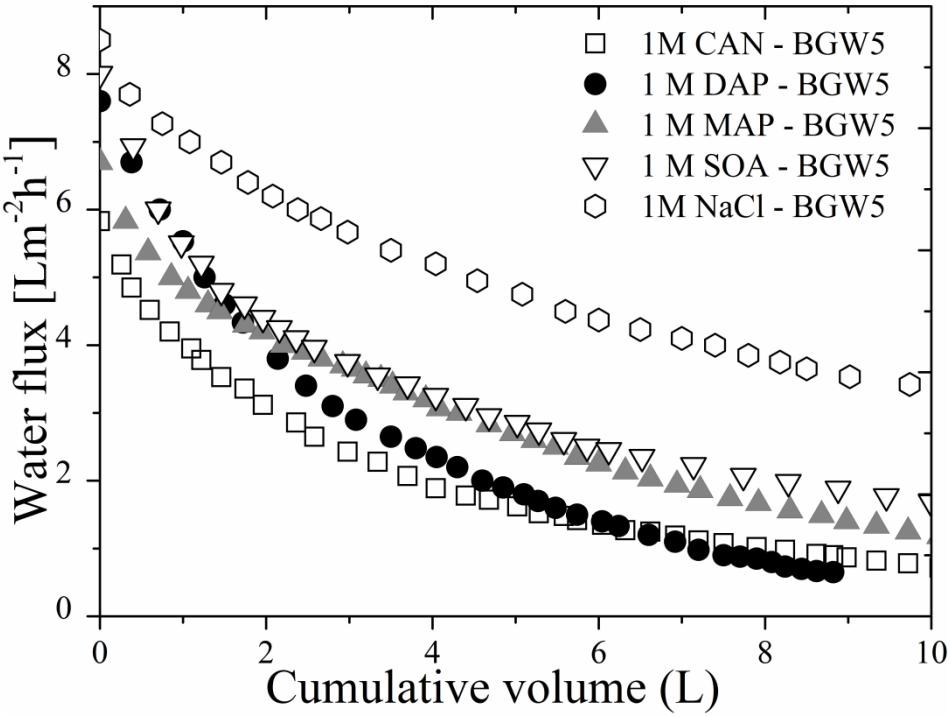
1M CAN - BGW5
1 M DAP - BGW5
1 M MAP - BGW5
1 M SOA - BGW5
1M NaCl - BGW5
Water flux [Lm-2h-1]
Cumulative volume (L)
0
2
4
6
8
10

(a)

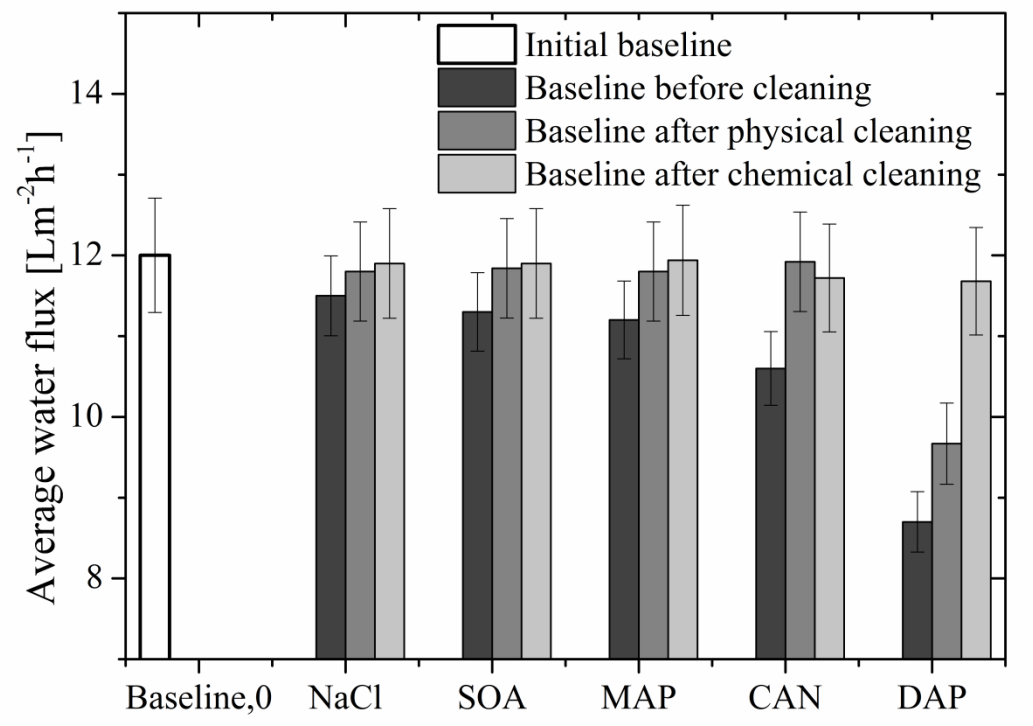
Initial baseline
Baseline before cleaning
Baseline after physical cleaning
Baseline after chemical cleaning
Average water flux [Lm-2h-1]
8
10
12
14
Baseline,0
NaCl
SOA
MAP
CAN
DAP

(b)

Figure 3

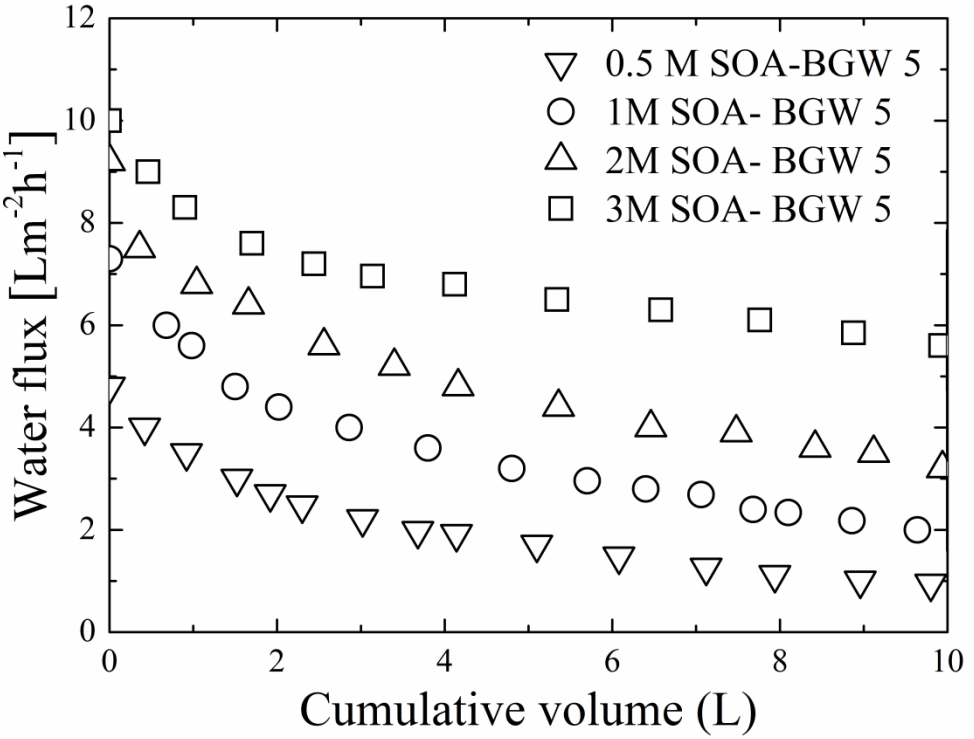
0.5 M SOA-BGW 5
1M SOA- BGW 5
2M SOA- BGW 5
3M SOA- BGW 5
Water flux [Lm-2h-1]
Cumulative volume (L)
0
2
4
6
8
10
12

(a)

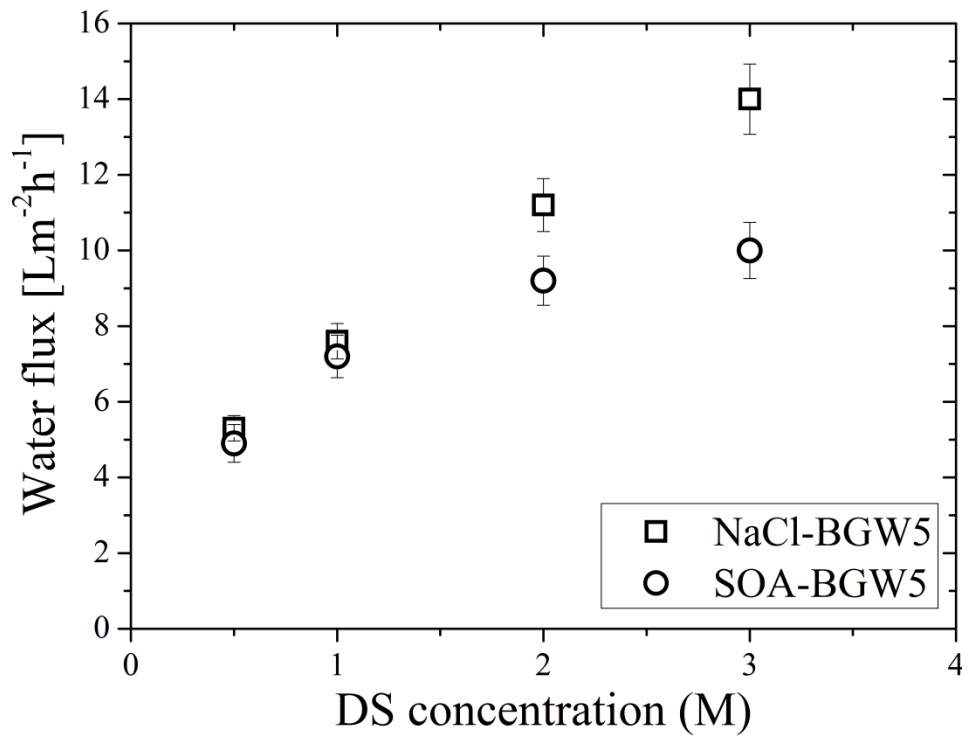
NaCl-BGW5
SOA-BGW5
Water flux [Lm-2h-1]
DS concentration (M)
0
1
2
3
4
0
2
4
6
8
10
12
14
16

(b)

Figure 4

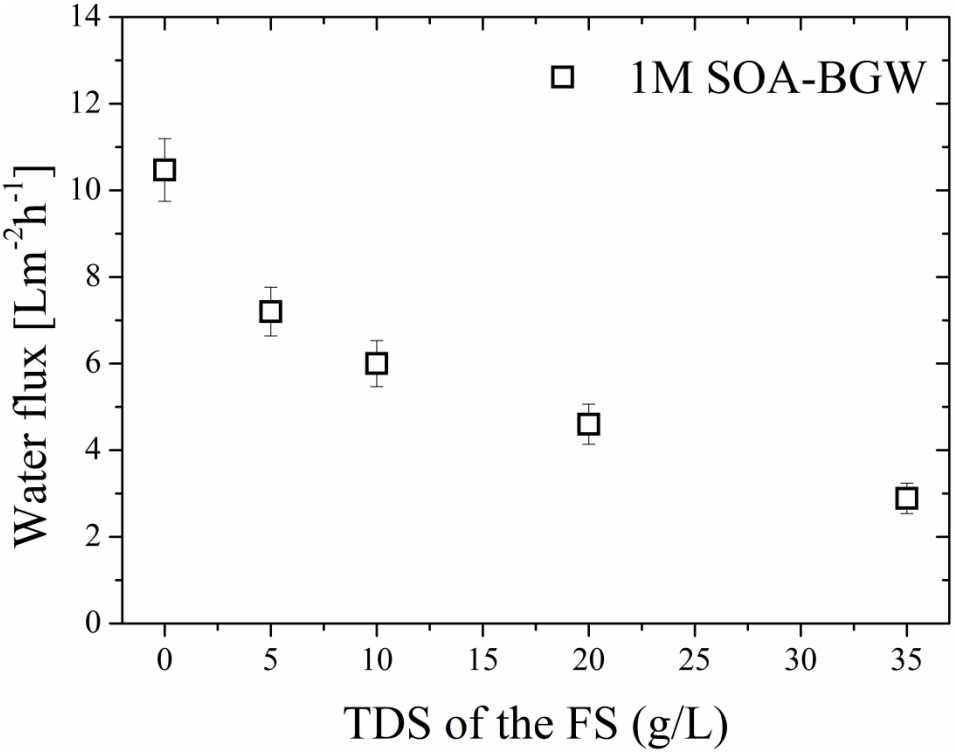
1M SOA-BGW
Water flux [Lm-2h-1]
TDS of the FS (g/L)
0
2
4
6
8
10
12
14
0
5
10
15
20
25
30
35

(a)

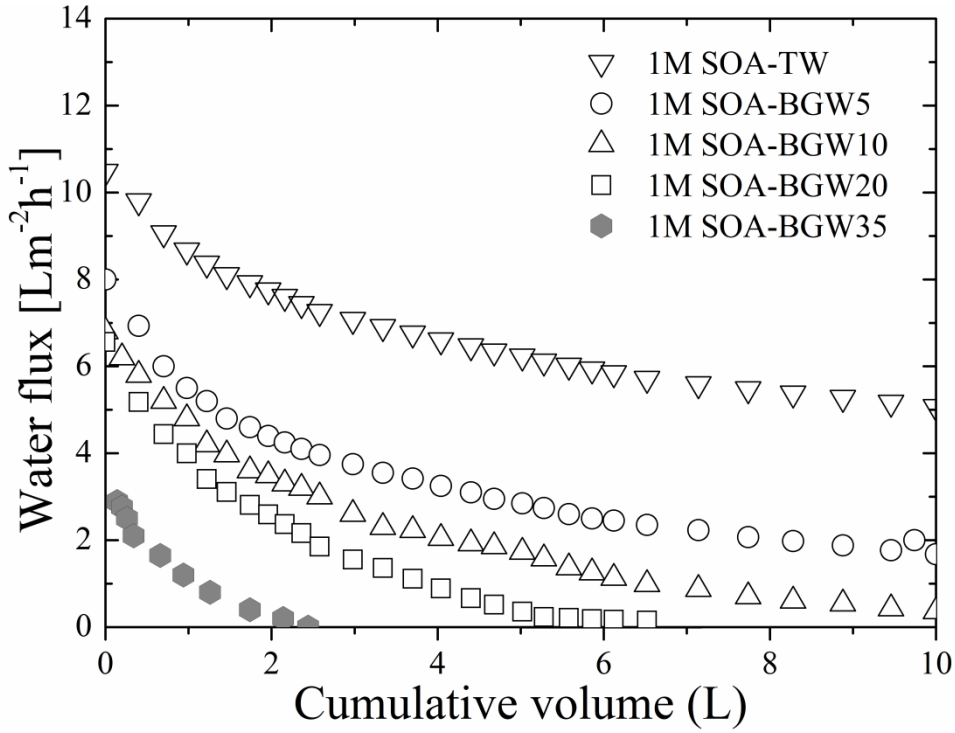
1M SOA-TW
1M SOA-BGW5
1M SOA-BGW10
1M SOA-BGW20
1M SOA-BGW35
Water flux [Lm-2h-1]
Cumulative volume (L)
0
2
4
6
8
10
12
14

(b)

Figure 5

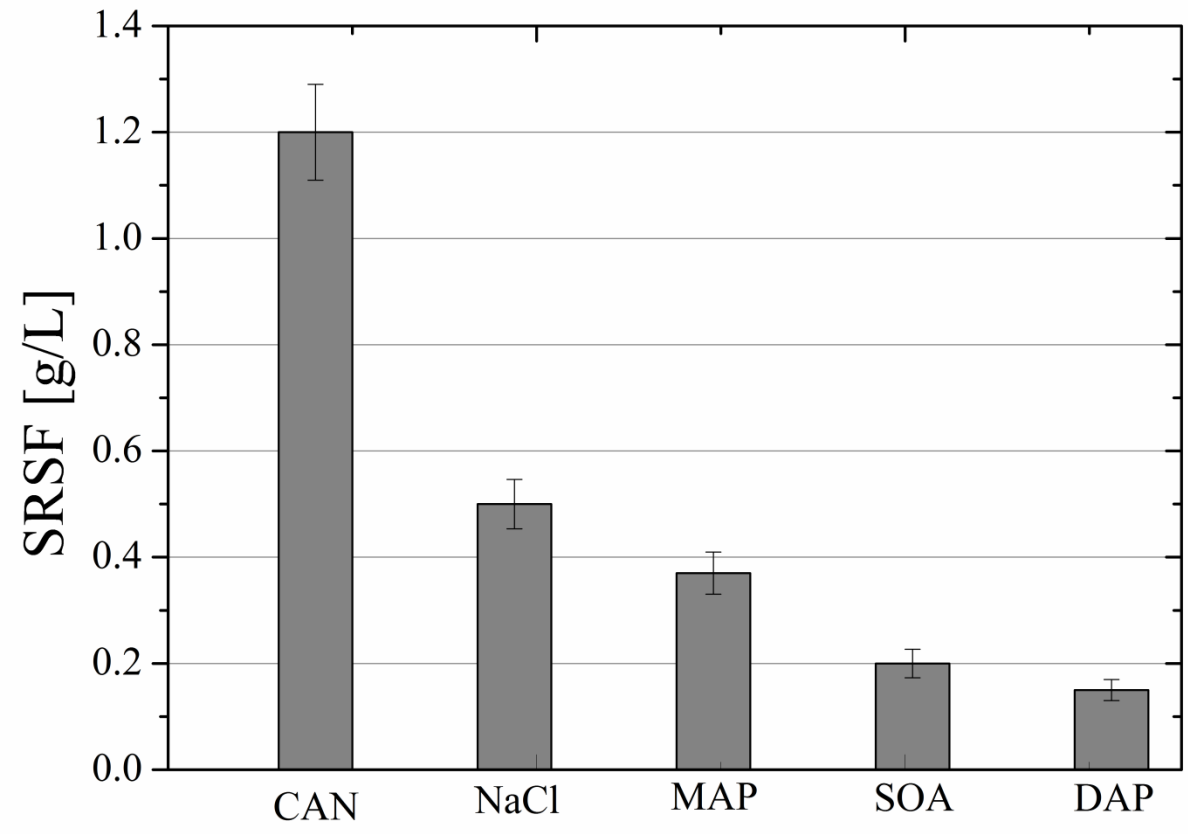

Figure 6

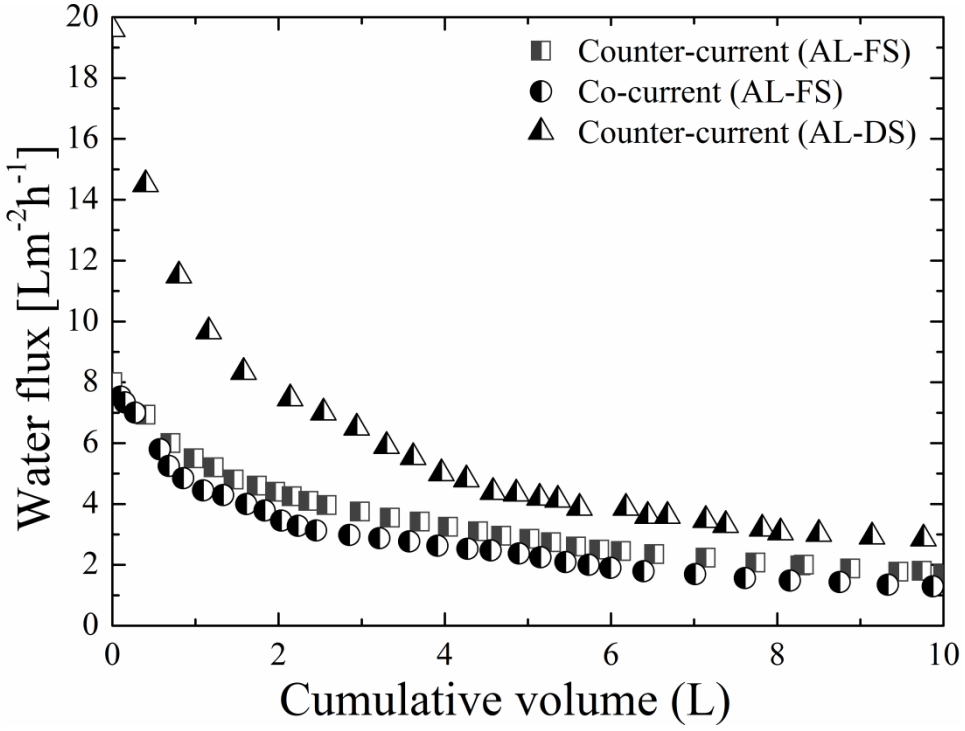
Counter-current (AL-FS)
Co-current (AL-FS)
Counter-current (AL-DS)
Water flux [Lm-2h-1]
Cumulative volume (L)
0
2
4
6
8
10
12
14
16
18
20

(a)

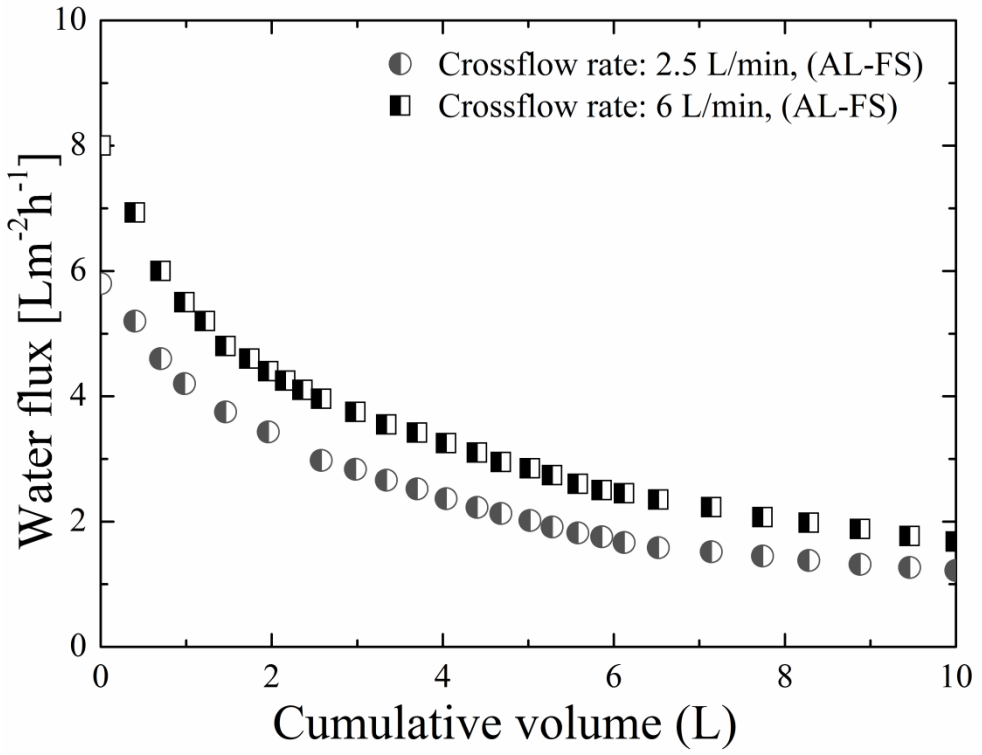
Crossflow rate: 2.5 L/min, (AL-FS)
Crossflow rate: 6 L/min, (AL-FS)
Water flux [Lm-2h-1]
Cumulative volume (L)
0
2
4
6
8
10

(b)

Figure 7